Sensitivity of Cyclone Tracks to the Initial Moisture Distribution: A Moist Potential Vorticity Perspective

Zuohao CAO[*1] and Da-Lin ZHANG[2]

[1] *Meteorological Service of Canada, Ontario, Canada*

[2] *Department of Meteorology, University of Maryland, College Park, Maryland, USA*

ABSTRACT

In this study, the characteristics of moist potential vorticity (MPV) in the vicinity of a surface cyclone center and their physical processes are investigated. A prognostic equation of surface absolute vorticity is then used to examine the relationship between the cyclone tracks and negative MPV (NMPV) using numerical simulations of the life cycle of an extratropical cyclone. It is shown that the MPV approach developed herein, i.e., by tracing the peak NMPV, can be used to help trace surface cyclones during their development and mature stages. Sensitivity experiments are conducted to investigate the impact of different initial moisture fields on the effectiveness of the MPV approach. It is found that the lifetime of NMPV depends mainly on the initial moisture field, the magnitude of condensational heating, and the advection of NMPV. When NMPV moves into a saturated environment at or near a cyclone center, it can trace better the evolution of the surface cyclone due to the conservative property of MPV. It is also shown that the NMPV generation is closely associated with the coupling of large potential temperature and moisture gradients as a result of frontogenesis processes. Analyses indicate that condensation, confluence and tilting play important but different roles in determining the NMPV generation. NMPV is generated mainly through the changes in the strength of baroclinicity and in the direction of the moisture gradient due to moist and/or dry air mass intrusion into the baroclinic zone.

Key words: cyclone tracks, moist potential vorticity, mid-latitude cyclones

1. Introduction

Extratropical cyclones are an important class of synoptic-scale weather systems. These systems play important roles not only in the long-term balances of energy, momentum, and water vapor in the climate system, but also in the regional weather and climate through changes in regional temperature and precipitation extremes (Cao et al., 2001, 2002, 2004). The North Atlantic-European and the North Pacific sectors are two typical regions in the Northern Hemisphere where weather and climate are significantly influenced by these synoptic-scale weather systems (Fraedrich et al., 1986; Gyakum et al., 1996). Despite the importance of these mobile cyclones in determining the large- and regional-scale weather and climate, our understanding of the fundamental processes leading to their development, maintenance, and termination is far from complete. Therefore, the objective of this study is to examine the sensitivity of cyclone tracks to physical processes associated with initial moisture distribution using the theory of the generation of negative moist potential vorticity (NMPV) by Cao and Zhang (2004).

The variable of MPV is chosen in this study to track cyclone movements due to its simple expression and its enriched three-dimensional (3-D) atmospheric information including dynamic, thermodynamic and moisture processes. The MPV is defined as

$$M_{\mathrm{PV}} = \frac{1}{\rho}\boldsymbol{\zeta}_{\mathrm{a}} \cdot \nabla\theta_{\mathrm{e}} , \qquad (1)$$

where $\boldsymbol{\zeta}_{\mathrm{a}}, \theta_{\mathrm{e}}$ and ρ are the absolute vorticity vector, equivalent potential temperature (Betts and Dugan, 1973) and density, respectively. Because MPV includes the moisture variable, it is different from potential vorticity (PV) (Hoskins et al., 1985; Davis and Emanuel, 1991; Huo et al., 1998) in terms of conservation and generation properties. MPV is conserved in a saturated atmosphere, and is generated in unsaturated regions of 3-D flows, but not in 2-D equatorial

*E-mail: zuohao.cao@ec.gc.ca

flows (Gao et al., 2004). In other words, MPV is conserved in the presence of condensational heating, but PV is not. As found by Cao and Cho (1995) (hereafter referred to as CC), negative (positive) MPV can be generated in regions where baroclinic vectors have a component along (against) the direction of moisture gradients. The observational studies of Thorpe and Clough (1991) have shown that MPV<0 can be more readily satisfied in the atmosphere than PV< 0. It has been shown in our previous study (Cao and Zhang, 2004) that NMPV can be a useful variable for tracing surface cyclones.

The next section presents a theoretical basis for using MPV to trace the movement of surface cyclones. Section 3 demonstrates the applicability of the theory using the numerical simulations of extratropical cyclones. The effects of perturbing the initial moisture distribution on the generation of NMPV and cyclone tracks will also be examined, and the kinematic and dynamic relations between NMPV and surface cyclone tracks will be diagnosed. A summary and conclusions are given in the final section.

2. Theory

Based on the primitive equation system, the prognostic equations for absolute vorticity and MPV in the absence of friction can be written as:

$$\frac{d\boldsymbol{\zeta}_{\mathrm{a}}}{dt} = (\boldsymbol{\zeta}_{\mathrm{a}} \cdot \nabla)\boldsymbol{v} - \boldsymbol{\zeta}_{\mathrm{a}}\nabla \cdot \boldsymbol{v} + \frac{(\nabla\rho \times \nabla p)}{\rho^2} , \quad (2)$$

and

$$\frac{d(M_{\mathrm{PV}})}{dt} = \left(\frac{\boldsymbol{\zeta}_{\mathrm{a}}}{\rho} \cdot \nabla\right)\frac{d\theta_{\mathrm{e}}}{dt} + \nabla\theta_{\mathrm{e}} \cdot \frac{(\nabla\rho \times \nabla p)}{\rho^3} , \quad (3)$$

where p and $\boldsymbol{v}$ are pressure and velocity, respectively.

The rate of change of surface absolute vorticity can then be formulated as a function of MPV from Eqs. (2) and (3) [see Cao and Zhang (2004) for more detail]. The final equation can be written as:

$$\int_{S_L} \frac{\theta_{\mathrm{e}}}{\rho}\frac{d\zeta_{\mathrm{a}}}{dt} \cdot ds = \int_{S-S_L} \frac{\theta_{\mathrm{e}}}{\rho}\frac{d\zeta_{\mathrm{a}}}{dt} \cdot d\boldsymbol{s}$$
$$- \oint_S \frac{\theta_{\mathrm{e}}}{\rho}[(\boldsymbol{\zeta}_{\mathrm{a}} \cdot \nabla)\boldsymbol{v} - \boldsymbol{\zeta}_{\mathrm{a}}\nabla \cdot \boldsymbol{v}] \cdot d\boldsymbol{s}$$
$$- \int_V \left[\frac{d(M_{\mathrm{PV}})}{dt} - \left(\frac{\boldsymbol{\zeta}_{\mathrm{a}}}{\rho} \cdot \nabla\right)\frac{d\theta_{\mathrm{e}}}{dt}\right] dv ,$$
$$(4)$$

where S denotes a surface surrounding the volume V,

$$\int_V \frac{d(M_{\mathrm{PV}})}{dt} dv$$

is the rate of change of MPV, or the generation of MPV, in the volume V (see Fig. 1).
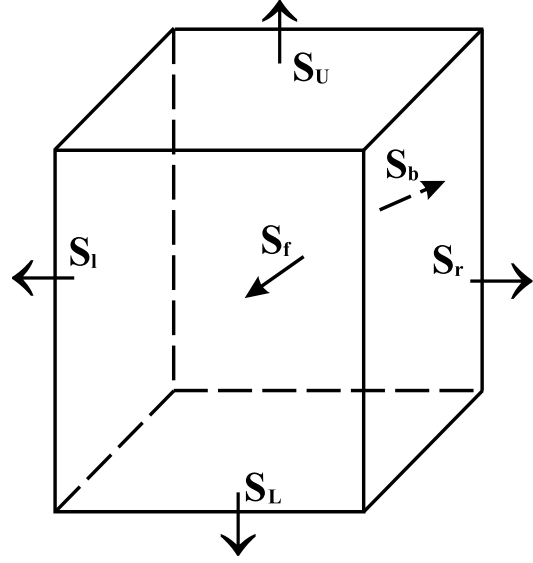

Fig. 1. A schematic diagram showing an integration over the volume V enclosed by the surface S, where $S = S_U + S_L + S_l + S_f + S_r + S_b$. The vectors indicate the normals perpendicular to the corresponding surfaces.

Equation (4) relates the rate of change of lower-level absolute vorticity to the rate of change of upper-level and lateral absolute vorticity, the tilting of absolute vorticity, and the divergence over the surface S, as well as the MPV generation in the atmospheric column. It is evident from Eqs. (2)–(4) that the lower-level absolute vorticity and the MPV generation in the atmospheric column can be linked through the common baroclinic source term, $(\nabla\rho \times \nabla p)/\rho^2$. In the PV framework, however, no such relationship can be derived between the lower-level absolute vorticity and the PV generation.

With the equation of state $p = \rho RT(1 + \alpha q)$ and the definition of potential temperature θ, the baroclinic source term in the absolute vorticity equation can be written as (CC)

$$\frac{(\nabla\rho \times p)}{\rho^2} = \frac{1}{\rho}\left[-\frac{1}{\theta}\nabla\theta \times \nabla p - \frac{\alpha}{1+\alpha q}\nabla q \times \nabla p\right] . \quad (5)$$

The last term in Eq. (4) is the same as the last term in Eq. (3), i.e., the generation of MPV due to the baroclinic-moisture effect. This term, denoted as

$$\left[\frac{d(M_{\mathrm{PV}})}{dt}\right]_{BM} ,$$

can be written as

$$\left[\frac{d(M_{\mathrm{PV}})}{dt}\right]_{BM} = A(\nabla\theta \times \nabla p) \cdot \nabla q$$
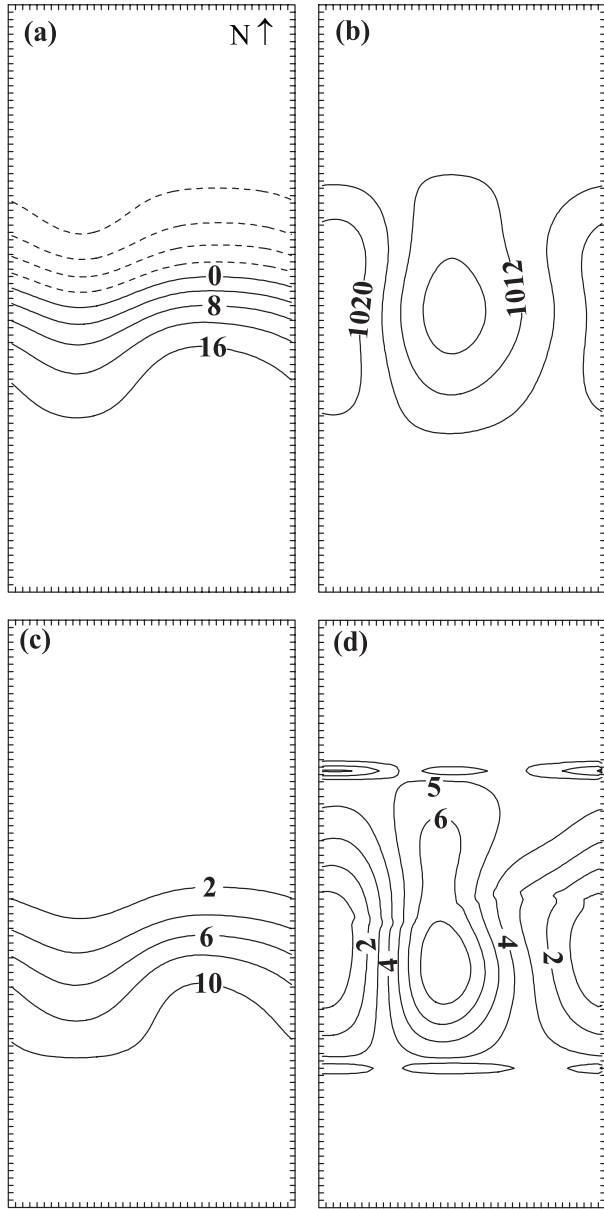$$= A(\nabla q \times \nabla p) \times (-\nabla\theta) , \quad (6)$$

Fig. 2. Horizontal distributions of the model initial conditions at the surface: (a) temperature at intervals of 4°C, (b) pressure at intervals of 4 hPa, (c) specific humidity at intervals of $2\,\mathrm{g\,kg^{-1}}$, and (d) MPV in the unit of 0.1 PVU. The abscissa is in the x direction and the ordinate is in the y direction. Here N↑ denotes North. The distance between two ticks is 100 km.

where A (see CC for details) is a function of $\theta, p,$ and q, and it has a negative value under typical atmospheric conditions (CC). Note that the baroclinic vector, $\nabla\theta \times \nabla p$, appears in both Eq. (5) and Eq. (6). The baroclinic vector in Eq. (5) contributes to the rate of change of absolute vorticity over a volume with an area of $|\nabla\theta \times \nabla p|$ and a unit depth whereas the contribution of the baroclinic vector in Eq. (6) is over
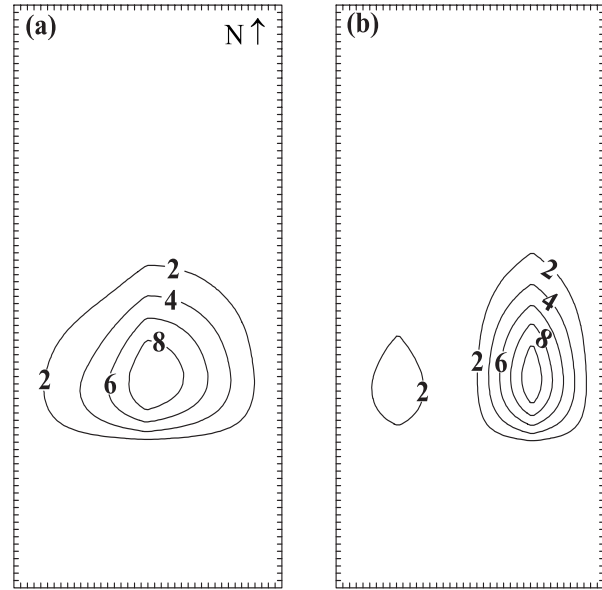

Fig. 3. The initial surface specific humidity fields, at intervals of $2\,\mathrm{g\,kg^{-1}}$, for (a) experiment A, and (b) experiment B.

a volume with an area of $|\nabla\theta \times \nabla p|$ and a depth of $|\nabla q| \cdot \cos\beta$, where β is an angle between the ∇q and the normal of $\nabla\theta \times \nabla p$. Therefore, the contribution of MPV generation to the rate of change of absolute vorticity is similar to that of the baroclinic vector, except for their different integration ranges in the vertical. If NMPV (positive MPV) is generated, it requires positive (negative) $(\nabla\theta \times \nabla p) \cdot \nabla q$, indicating that the baroclinicity increases (decreases) in the direction of moisture gradients. Hence, the NMPV generation contributes to the rate of change of absolute vorticity. Similar analyses can be performed for the vector $\nabla q \times \nabla p$ in both Eq. (5) and Eq. (6).

3. Application to the model simulated cyclones

Since MPV is nonlinearly related to the surface absolute vorticity, it is not possible to analytically obtain an explicit relationship between the two variables. In the previous study (Cao and Zhang, 2004), NMPV was used to track the evolution of an observed surface cyclone characterized with explosive lee cyclogenesis (Hu and Reiter, 1987), particularly during the period in which the surface cyclone signal was absent due to the blocking of the Rocky Mountains. In this paper, we will use model-simulated cyclones to test the applicability of the theory described in the preceding section. Note that our purpose is to use the NMPV to track/detect their displacements, so it is not necessary to calculate the budget of Eq. (4).
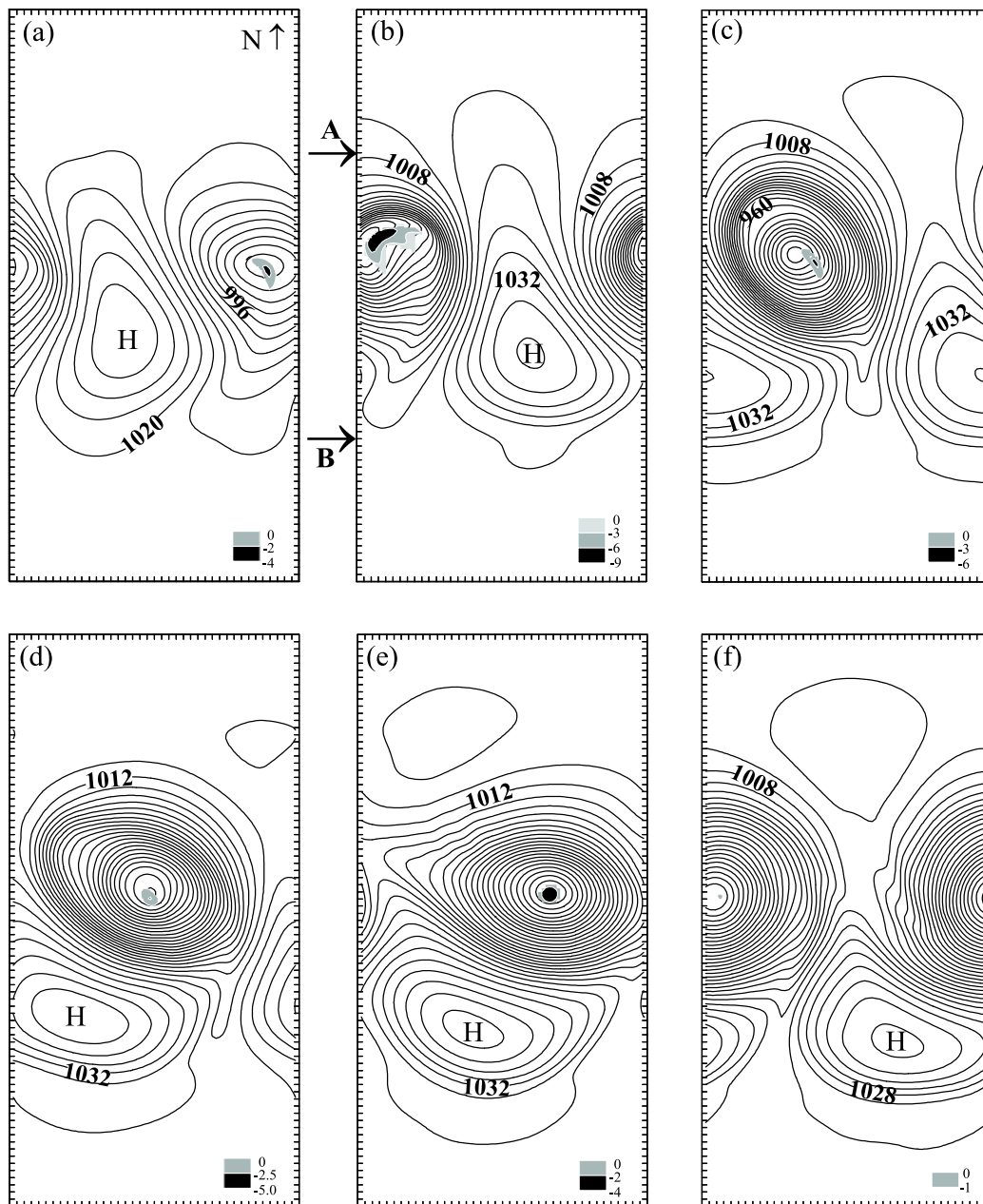
Fig. 4. Surface pressure (contours) at intervals of 4 hPa and the peak NMPV (shading) in the unit of 0.1 PVU for the control experiment at (a) 30 h on the 619-hPa pressure surface, (b) 48 h on the 817-hPa pressure surface, (c) 72 h on the 817-hPa pressure surface, (d) 84 h on the 689-hPa pressure surface, (e) 96 h on the 689-hPa pressure surface, and (f) 120 h on the 757-hPa pressure surface.

3.1 Model description and experiment design

The simulations of extratropical cyclones are obtained using the Penn State University-National Center for Atmospheric Research (PSU-NCAR) 3-D mesoscale model (Anthes et al., 1987). This model has been modified by CC to make it suitable for simu-

lating baroclinic channeled flows with periodic boundary conditions at the east and west boundaries and rigid-wall boundary conditions at the north and south boundaries. The horizontal domain size is 4000 km in the east-west (x) direction and 8000 km in the north-south (y) direction with a horizontal grid spacing of 50 km. The vertical σ-coordinate is used:
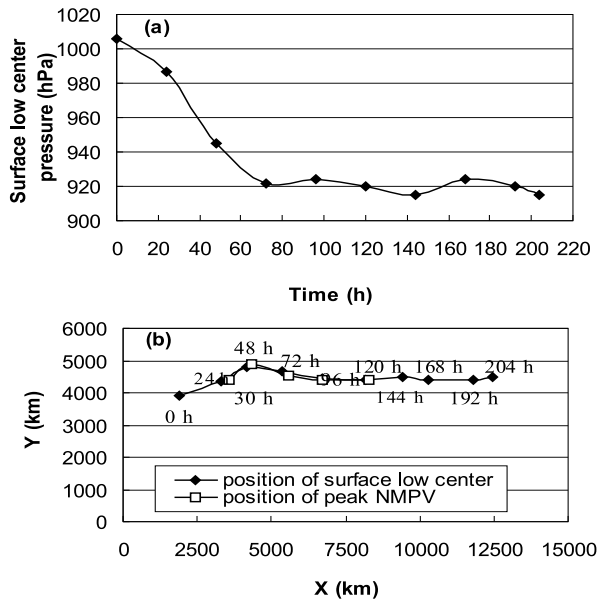
Fig. 5. (a) Time series of the surface cyclone center pressure (hPa), and (b) the tracks of the surface cyclone center at the hours of 0, 24, 48, 72, 96, 120, 168, 192, and 204, and the peak NMPV for the control experiment at the hours of 30, 48, 72, 96, and 120. The position of the peak NMPV (the surface cyclone center) in panel (b) is the distance between the peak NMPV center (the surface cyclone center) and the bottom left corner of the simulation domain.

$$\sigma = \frac{p - p_t}{p_s - p_t} \,, \tag{7}$$

where p_t(=300 hPa) and p_s are the top and the surface pressures of the model, respectively. The model consists of 14 computational layers at σ=0.996, 0.986, 0.960, 0.920, 0.870, 0.805, 0.730, 0.645, 0.550, 0.450, 0.350, 0.250, 0.150 and 0.050. The model physical processes include explicit calculations of cloud water and rain water as time-dependent variables (Hsie et al., 1984) and virtual temperature and water loading effects. The reader is referred to CC for detailed descriptions of the model features used in this study.

The initial surface conditions for the control run are given in Fig. 2, which shows a perturbation with moderate amplitude representing the early phase of typical mid-latitude cyclogenesis. Most of the surface meridional temperature gradients are localized in a 1250-km baroclinic zone (Fig. 2a). The specific humidity field varies from 1 to 10 g kg^{-1} (Fig. 2c), and the initial moisture gradients are more or less parallel to the potential temperature gradients (cf. Figs. 2c and 2a). The initial MPV is positive everywhere in the domain (Fig. 2d) and thus the model atmosphere is conditionally symmetrically stable. Interested readers are referred to CC for details.

Two sensitivity experiments are conducted to investigate the effects of initial moisture distributions on both the NMPV generation and surface cyclone tracks. In each experiment, a different initial moisture distribution is specified (Fig. 3) while all the other model initial conditions are held the same as in the control experiment. As compared to the control run, components of moisture gradients perpendicular to temperature gradients are introduced in experiments A and B. In experiment A, a high specific humidity is specified in the warm sector, as is frequently observed (e.g., Bennetts and Ryder, 1984), whereas in experiment B, the high moisture content is specified ahead of the surface low pressure center. Note that the specified moisture distributions are motivated by conceptual considerations rather than realistic cases although they are qualitatively similar to some realistic situations. In both sensitivity runs, the initial MPV is again positive everywhere in the domain.

3.2 *Life cycle of extratropical cyclones*

The PSU-NCAR model is integrated for 8.5 days to simulate the life cycle of a mid-latitude cyclone. The simulated surface temperature field from the control run shows many typical features of mid-latitude cyclogenesis, such as the warm conveyor belt, the bent-back warm front and the T-bone structure, and the seclusion of the warm core enclosed by the 0°C isotherm (Fig. 2 of CC). The simulated life cycle is similar to that of Shapiro and Keyser's (1990) and agrees very well with observational studies by Neiman and Shapiro (1993) and Neiman et al. (1993).

The control-simulated cyclone experiences significant changes in surface pressure during its life cycle (Figs. 4 and 5). Figure 5 provides the time series of surface pressure at the cyclone center and the track of the surface low center (defined here as the position of minimum surface pressure). The surface cyclone deepens rapidly from 1006 to 922 hPa in the first 72 h, at an average rate of 1.17 hPa h^{-1} (Fig. 5a). It reaches 915 hPa at the end of the 144-h integration. During the first 48 h, it moves northeastward with a meridional displacement of 900 km and a zonal displacement of 2250 km (Fig. 5b). This traveling speed is comparable to some observed speeds (e.g., see Szeto et al., 1999). During the next 48 h after reaching the mature stage, the cyclone moves southeastward with meridional and zonal displacements of 350 km and 2550 km, respectively. After 96 h, the surface cyclone moves eastward with fluctuations in the meridional directions.

In contrast, the averaged deepening rates in experiments A and B during the first 72 h are about 1.03 hPa h^{-1} and 1.0 hPa h^{-1}, respectively (Figs. 6a and
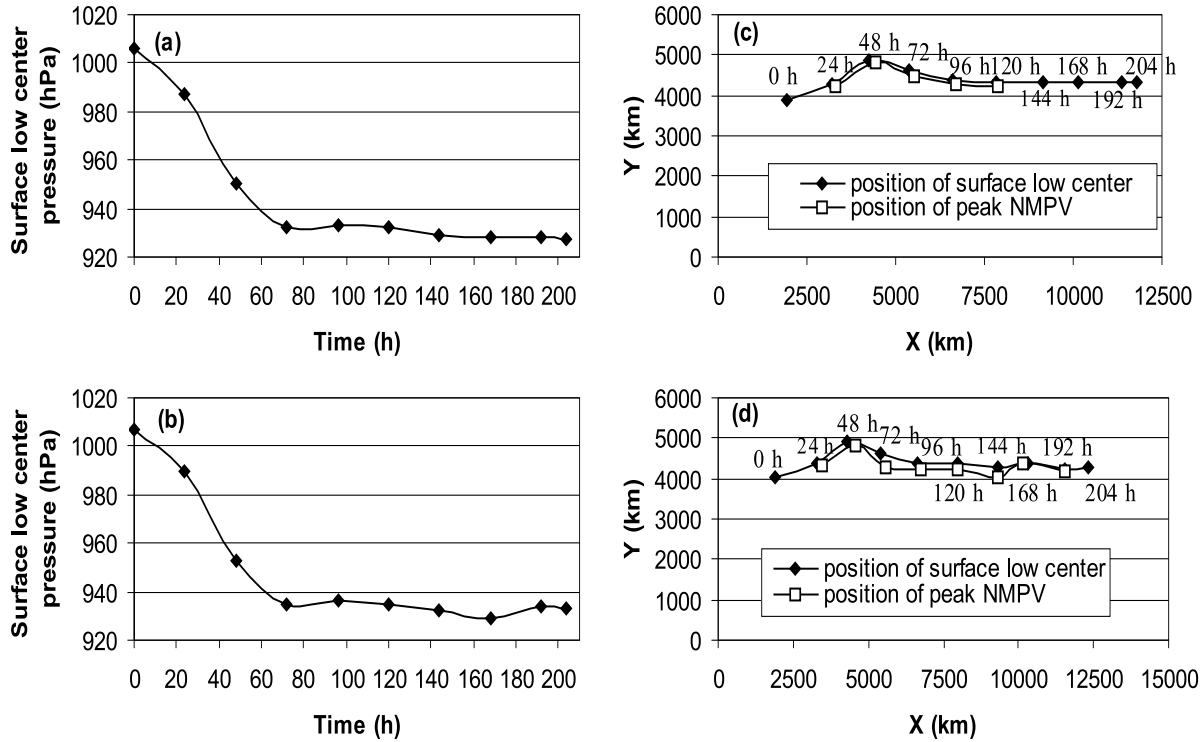
Fig. 6. Time series of the surface cyclone center pressure (hPa) for (a) experiment A, and (b) experiment B, and the tracks of the surface cyclone center and the peak NMPV for (c) experiment A, and (d) experiment B. The position of the peak NMPV (the surface cyclone center) in panels (c) and (d) is the distance between the peak NMPV center (the surface cyclone center) and the bottom left corner of the simulation domain.

6b). The displacements of the two simulated cyclones are similar to the control one during the first 96 h. For example, in the first 48 h, the cyclones in experiments A and B have meridional displacements of 950 km and 850 km and zonal displacements of 2300 km and 2400 km, respectively, whereas in the second 48 h, they have meridional displacements of 450 km and 500 km and the same zonal displacement of 2350 km. After 120 h, the cyclone in experiment A moves eastward whereas the cyclone simulated in experiment B fluctuates in the meridional directions (Figs. 6c and 6d).

It should be mentioned that although latent heat release is not a necessary condition for cyclogenesis (Uccellini, 1990), it plays an important role in enhancing cyclogenesis. For instance, Gyakum (1983) and Roebber (1984) suggested that the preferred regions of explosive cyclogenesis are primarily baroclinic zones and that convection and baroclinic processes are the explosive forcing mechanism. Colle and Mass (1999) found thatdiabatic effects are important in maintaining baroclinic systems in mountainous regions. Based on the compiled statistics of 15 oceanic cyclones, Reed et al. (1993) found that latent heat release, on average, increased the 24-h deepening rate by a factor of 2.

All of our experiments show that these cyclones experience explosive deepening at rates that are much higher than those in the corresponding dry experiments (not shown).

3.3 *Surface cyclone tracks and the MPV kinematics*

It is evident from Fig. 5b that during the first 48 h the control-simulated cyclone tends to move northeastward, namely, from warm-moist to cold-dry areas. This movement helps convert potential energy stored in the baroclinic zones into kinetic energy, and condense the moist air in drier and colder environments, both favoring the cyclogenesis. This can be interpreted in terms of the MPV generation in Eq. (6), i.e.,

$$\left[\frac{d}{dt}(M_{\mathrm{PV}})\right]_{BM} = A(\nabla\theta \times \nabla p) \cdot \nabla q$$
$$= A\left(-\nabla_p\theta \times \frac{\partial p}{\partial n}\boldsymbol{n}\right) \cdot (-\nabla_{\mathrm{p}}q), \quad (8)$$

where ∇_{p} is a horizontal gradient operator on a constant pressure surface and $\boldsymbol{n}$ is the unit vector normal to the pressure surface. Hence, NMPV can be generated in the unsaturated regions where baroclinic vec-
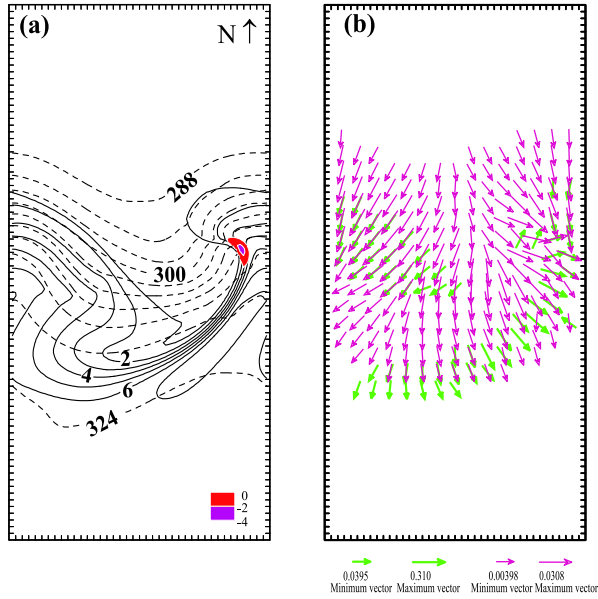
Fig. 7. (a) Horizontal distribution of specific humidity (solid contours) at intervals of $1 \, \mathrm{g \, kg^{-1}}$ and potential temperature (dashed contours) at intervals of 4 K, superposed with NMPV in the unit of 0.1 PVU, and (b) horizontal vectors of specific humidity gradients (green; each component scaled by a factor of $10^{-7} \, \mathrm{m^{-1}}$) and potential temperature gradients (red; each component scaled by a factor of 10^{-3} $\mathrm{K \, m^{-1}}$) on the 619-hPa pressure surface at 30 h of the control simulation.

tors, $\nabla\theta \times \nabla\mathrm{p}$, have a component along the direction of the moisture gradients. If the θ gradient vectors are perpendicular to the q gradient vectors, the MPV generation will be maximized for a given $\nabla\mathrm{p}$. For example, in experiment A, the high specific humidity is specified in the warm sector, as is frequently observed (Bennetts and Ryder, 1984), so the MPV generation can be maximized through the intersection of the θ and q gradient vectors in the warm sector.

To examine the relationship between NMPV and surface cyclone tracks, we first calculate the 3-D MPV field from the model output, and then search for the peak NMPV in the vertical, and plot NMPV at that level. Finally, the center of the peak NMPV on that level is positioned, and considered as the cyclone center. It is encouraging from Figs. 4 and 5b that the peak NMPV centers provide a good tracking of the cyclone movements at different stages of its development (up to 5 days). After day 5, NMPV disappears mainly due to the presence of positive MPV generation.

A further examination indicates that the peak NMPV centers are closely associated with the displacements of air masses with large θ and q gradients. For example, at 30 h, a moist tongue extends from the warm sector into the cyclone center where NMPV first
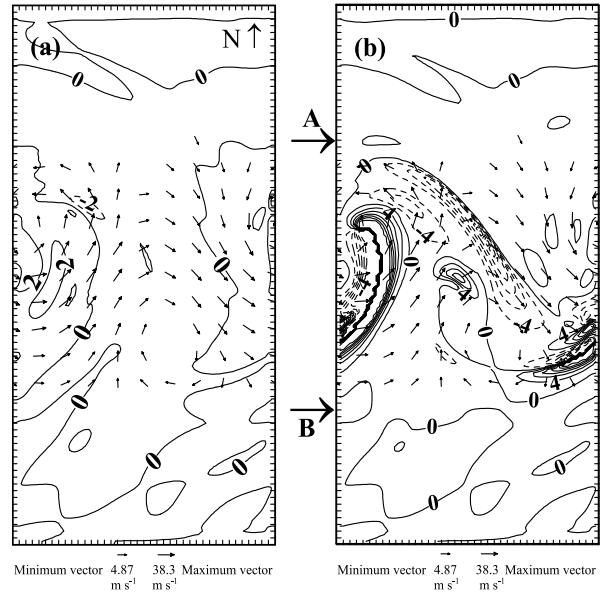
Fig. 8. Horizontal distribution of (a) $\boldsymbol{v} \cdot \nabla\theta/\theta$ at intervals of $2\times10^{-6} \, \mathrm{s^{-1}}$, and (b) $\boldsymbol{v} \cdot \nabla q/q$ at intervals of 4×10^{-5} $\mathrm{s^{-1}}$, superposed with horizontal velocity vectors, on the 757-hPa pressure surface at 48 h of the control simulation.

appears as a result of the significant changes of q gradients in the baroclinic zones (Figs. 7a and 7b). Of particular importance is that the θ gradient vectors are nearly perpendicular to the q gradient vectors over the peak NMPV regions. Similar scenarios also occur at the other times. Likewise, the θ advection into the regions of high q gradients favors the NMPV generation. To see the relative significance of the q advection into the regions of high θ gradients and vice versa, the θ and q advections are calculated and divided by θ and q, respectively, in order to compare them based on the same dimension (i.e., $\mathrm{s^{-1}}$). A comparison between Figs. 8a and 8b indicates that at the mature stage, the q advection is about one order of magnitude greater than the θ advection, which is in agreement with the observations of Cao and Moore (1998). At 48 h, positive q advection occurs mostly along the cold front where horizontal wind shears are present, and along the bent-back warm front (Fig. 8b). The strong negative q advection can also be observed next to the positive q advection. In contrast, the θ advection is positive adjacent to the cold front and negative near the bent-back warm front (Fig. 8a). The above results indicate that the displacements of large θ and q gradients, which are favorable for the NMPV generation, are mainly realized through the intrusion of moist and/or dry air into strong baroclinic zones.

It is evident from Eq. (8) that the NMPV generation occurs mostly in regions where a component of $\nabla_{\mathrm{p}}\theta$ is perpendicular to $\nabla_{\mathrm{p}}q$, as is also shown in
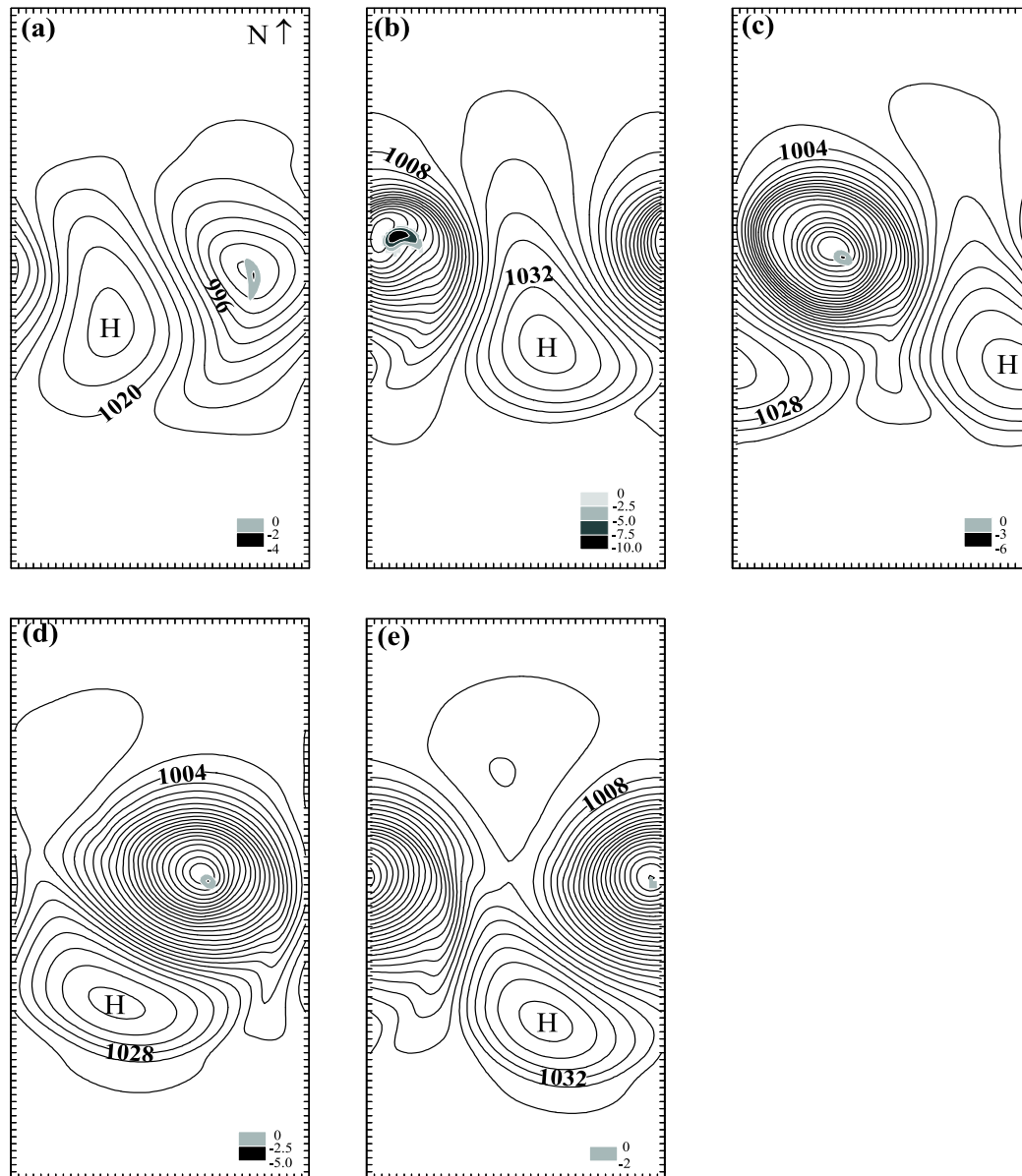
Fig. 9. Same as Fig. 4, except for experiment A: (a) at 24 h on the 619-hPa pressure surface, (b) at 48 h on the 817-hPa pressure surface, (c) at 72 h, (d) at 96 h, and (e) at 120 h on the 757-hPa pressure surface.

Figs. 7a and 7b. This can be realized through (a) initial specifications of the θ and q gradients in an unsaturated environment, (b) condensational heating induced θ and q gradients in the vicinity of saturated regions, and (c) nonlinear advective processes. Because of these factors, the location of peak NMPV changes from one level to another during the life cycle of extratropical cyclones. In the present study, the peak NMPV is located between 871 hPa and 619 hPa in all the simulations conducted herein. The location is similar to the peak mass-weighted NMPV integrated from 871 to 619 hPa, indicating their nearly vertically-coherent structures.

Experiments A and B can also be used to understand the impact of perturbing the initial moisture field on the generation of NMPV. When higher specific humidity is distributed in the warm sector (Expt. A), its gradients are mostly perpendicular to the θ gradients (Fig. 3a). This results in the initial MPV sources being greater than those in the control experiment (not shown). Nevertheless, the peak NMPV can still act as a good indicator of the surface cyclone movement up
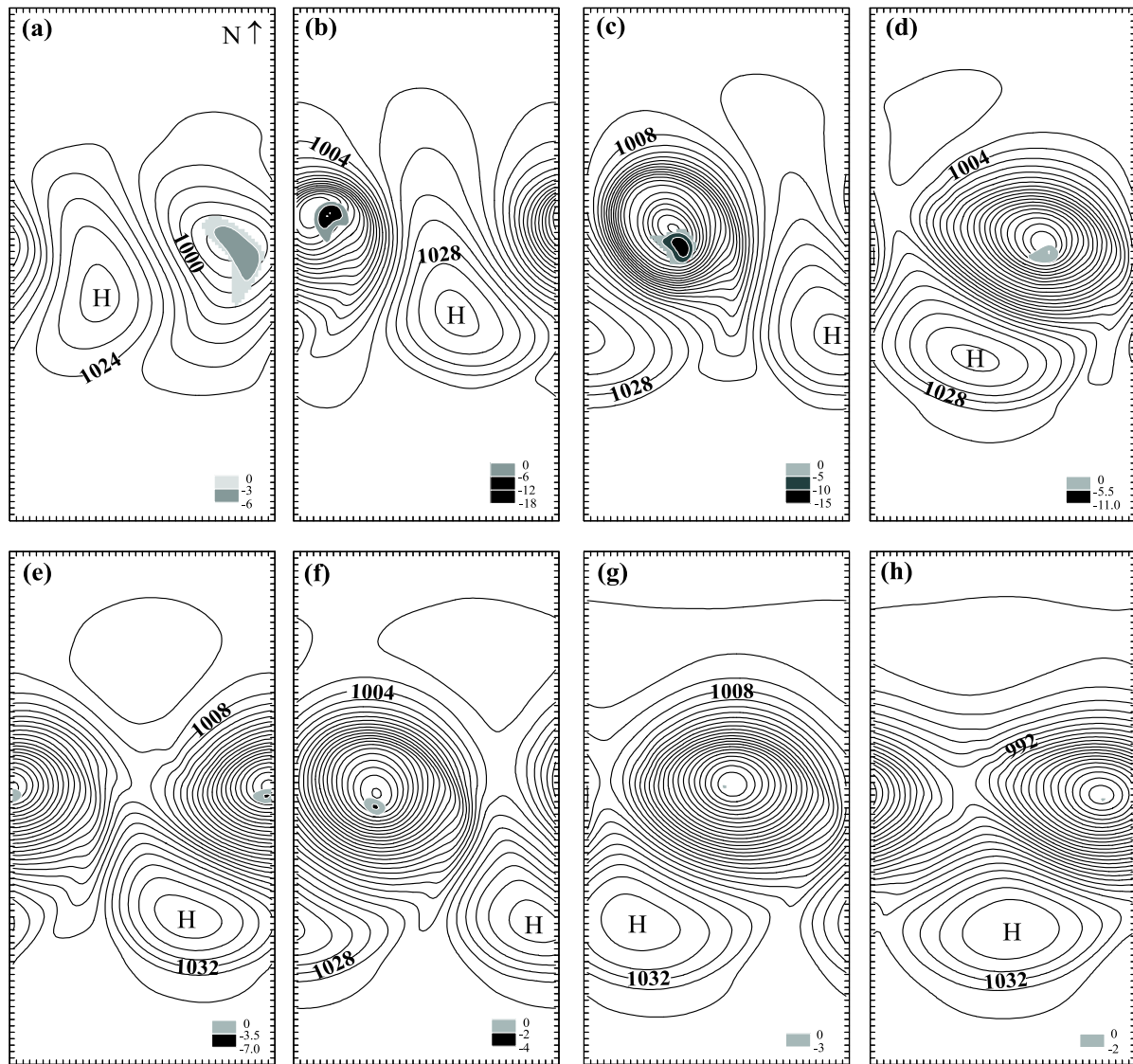
Fig. 10. Same as Fig. 4, except for experiment B: (a) at 24 h on the 757-hPa pressure surface, (b) at 48 h on the 871-hPa pressure surface, (c) at 72 h, (d) at 96 h, (e) at 120 h, (f) at 144 h, (g) at 168 h, and (h) at 192 h on the 817-hPa pressure surface.

to 5 days (see Figs. 9 and 6c). When higher specific humidity is located ahead of the surface low with the θ and q gradient vectors normal to each other (Fig. 3b), the initial MPV sources are higher than those in the control run (not shown) due to the orientation of the initial moisture gradients. As a result, NMPV in experiment B persists the longest (up to 8 days) as a tracer of the surface cyclone (Figs. 10 and 6d), as compared to that in the control (up to 5 days) and experiment A (cf. Figs. 4 and 5b, and Figs. 9 and 6c).

As mentioned earlier, MPV cannot be generated or destroyed in the presence of latent heat release, but NMPV can be generated in the vicinity of con-densation areas where the existing θ and q gradient vectors are significantly altered in either magnitude or direction (Cao and Moore, 1998). Hence, NMPV tends to be generated near the cyclone center where two major condensation regions overlap. This can be further seen from the evolution of the simulated cloud field. At the early stage of cyclogenesis, a "baroclinic leaf" (Weldon, 1979) appears at the northern end of the warm conveyor belt, and NMPV is generated to the west of the "baroclinic leaf" near the cyclone cen-ter (cf. Figs. 11a and 4a). At the mature stage, a comma-shaped cloud, which resembles remarkably the satellite-observed clouds (Browning, 1990), is formed

and latent heat release is increased (Fig. 11b). At this stage, the magnitude of NMPV is increased at the inner edge of the comma-shaped cloud due to the enhanced θ and q gradients in the vicinity of condensation areas. Meanwhile, NMPV begins to appear along the cold front. Note that the NMPV presented in Fig. 11 occurs at a level that is different from the level of the peak NMPV.

The effects of condensation on the NMPV generation can also be observed from experiments A and B. For example, the peak NMPV first appears near the cyclone center which is next to the saturated areas (Figs. 9a and 10a). Adjacent to the condensational regions, baroclinicity and moisture gradients increase, amplifying the NMPV generation and enhancing the cyclogenesis (Figs. 9b and 10b).

When NMPV is advected into saturated regions, it becomes a more useful variable for tracking surface cyclones due to its conservation property. Thus, the effective time scale to track surface cyclones depends on the distribution and magnitude of initial moisture content and the strength of vertical motion induced by condensational heating. As found in Zhang (2003), organized upward motion is well correlated with large areas of cloud development. Figure 12 shows that the total latent heat release in the control experiment is much greater than that in Expts. A and B because of the larger domain-integrated moisture content (Fig. 13). By comparison, the peak NMPV in Expt. B can persist longer (8 days) than that in the control (5 days) for tracking the cyclones.

3.4 Development of large θ and q gradients

In view of the important roles of the highly correlated large θ and q gradients in the NMPV generation, it is desirable to examine the processes leading to the development of these large gradients. The rate of change of the θ gradients on a constant pressure surface, i.e., the frontogenesis function (Petterssen, 1936), can be expressed as:

$$F = \frac{1}{|\nabla_{\mathrm{p}}\theta|} \left[\underbrace{-\frac{\partial \theta}{\partial x}\left(\frac{\partial u}{\partial x}\frac{\partial \theta}{\partial x} + \frac{\partial v}{\partial x}\frac{\partial \theta}{\partial y}\right) - \frac{\partial \theta}{\partial y}\left(\frac{\partial u}{\partial y}\frac{\partial \theta}{\partial x} + \frac{\partial v}{\partial y}\frac{\partial \theta}{\partial y}\right)}_{(\mathrm{I})} \right.$$
$$\left. \underbrace{-\frac{\partial \theta}{\partial x}\left(\frac{\partial \omega}{\partial x}\frac{\partial \theta}{\partial p}\right) - \frac{\partial \theta}{\partial y}\left(\frac{\partial \omega}{\partial y}\frac{\partial \theta}{\partial p}\right)}_{(\mathrm{II})} + \underbrace{\frac{\pi}{c_p}\frac{\partial \theta}{\partial x}\frac{\partial \dot{Q}}{\partial x} + \frac{\pi}{c_p}\frac{\partial \theta}{\partial y}\frac{\partial \dot{Q}}{\partial y}}_{(\mathrm{III})} \right], \tag{9}$$

where $\dot{Q}$ is diabatic heating and π is the exner pressure.

Similarly, the rate of change of the q gradients $d|\nabla_{\mathrm{p}}q|/dt$ (referred to as function M hereafter) on a constant pressure surface can be expressed as (Cao and Moore, 1998):

$$M = \frac{1}{|\nabla_{\mathrm{p}}q|} \left[\underbrace{-\frac{\partial q}{\partial x}\left(\frac{\partial u}{\partial x}\frac{\partial q}{\partial x} + \frac{\partial v}{\partial x}\frac{\partial q}{\partial y}\right) - \frac{\partial q}{\partial y}\left(\frac{\partial u}{\partial y}\frac{\partial q}{\partial x} + \frac{\partial v}{\partial y}\frac{\partial q}{\partial y}\right)}_{(\mathrm{I})} \right.$$
$$\left. \underbrace{-\frac{\partial q}{\partial x}\left(\frac{\partial \omega}{\partial x}\frac{\partial q}{\partial p}\right) - \frac{\partial q}{\partial y}\left(\frac{\partial \omega}{\partial y}\frac{\partial q}{\partial p}\right)}_{(\mathrm{II})} \underbrace{-\frac{1}{L}\frac{\partial q}{\partial x}\frac{\partial \dot{Q}}{\partial x} - \frac{1}{L}\frac{\partial q}{\partial y}\frac{\partial \dot{Q}}{\partial y}}_{(\mathrm{III})} \right]. \tag{10}$$

Functions F and M include the effects of the confluence due to convergence and horizontal (nondivergent) deformation (I), the tilting of the vertical gradients in θ and q onto the horizontal (II), and the horizontal variations of diabatic heating or cooling (III).

Qualitatively, cold (dry) advection on the cold (dry) side and warm (moist) advection on the warm (moist) side tends to increase the θ (q) gradient. Rising motion on the warm (moist) side and sinking motion on the cold (less moist) side decrease (increase) the horizontal
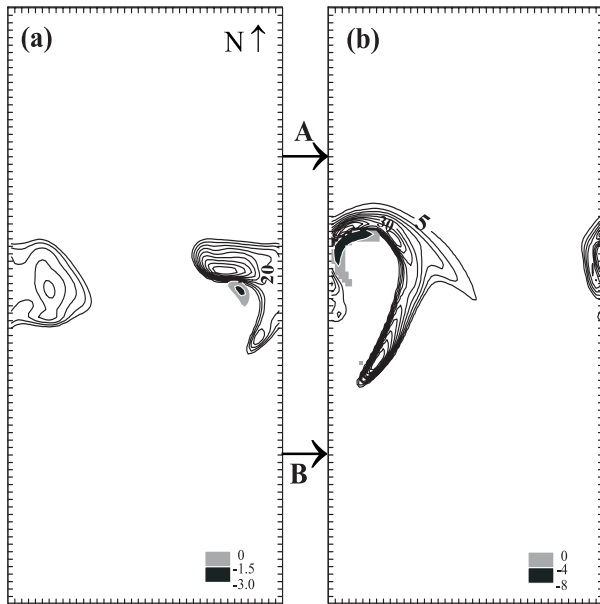
Fig. 11. Cloud water content (contours) at intervals of 5×10^{-5} g kg^{-1} and NMPV fields (shading) in the unit of 0.1 PVU for the control experiment at (a) 30 h and (b) 48 h on the 757-hPa pressure surface.
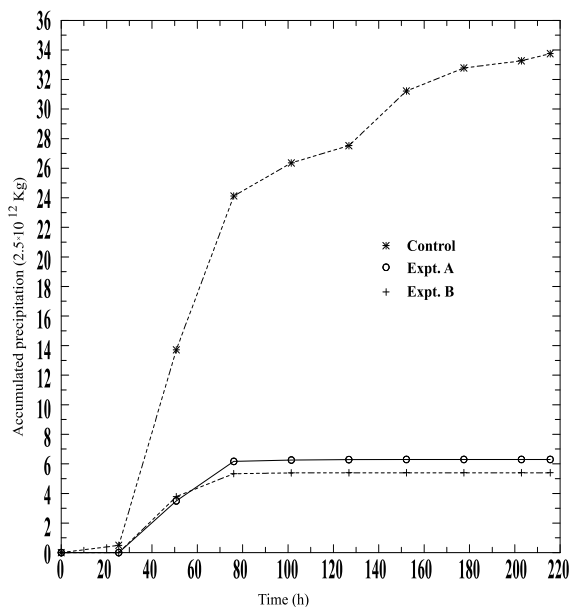

Fig. 12. Time series of the domain-integrated accumulated precipitation (kg) for the control, and experiments A and B.

$\theta(q)$ gradient. Condensation on the warm (moist) side increases (decreases) the $\theta(q)$ gradient while condensation on the cold (less moist) side decreases (increases) the $\theta(q)$ gradient.

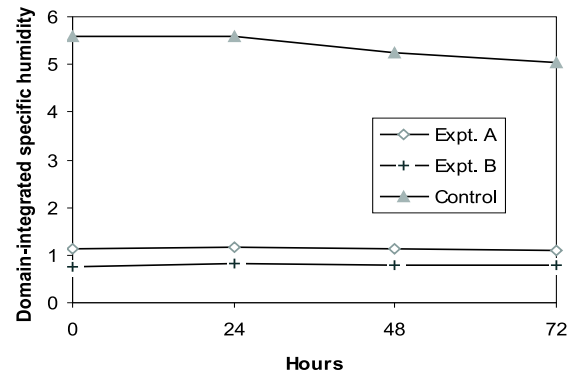**Fig. 13.** Time series of the domain-integrated specific humidity (scaled by a factor of 2.5×10^{14} kg) for experiments A and B and the control.

Figures 14a–c show that the contributions of confluence, tilting, and condensation to the rate of change of the θ gradients are of the same order of magnitude. It is evident that the θ gradient increases along the bent-back warm front due to the presence of strong confluence (Fig. 14a). Negative contributions, resulting mainly from the tilting effect, are also evident over almost the entire cyclone (Fig. 14b). Condensation takes place along the cold and the bent-back warm frontal regions (Fig. 12b), where significant positive and negative contributions in banded forms are observed (Fig. 14c).

Similarly, Figs. 14e–g show the contributions of the three processes to function M. Although they are of the same order of magnitude, the condensational effect is more important in determining the rate of change of the q gradients. The effects of confluence and tilting only appear along the southern and northern ends of the cold front, respectively (Figs. 14e and 14f), whereas the condensation effect is important along both the cold and the bent-back warm fronts (Fig. 14g).

A comparison between Figs. 14c and 14g shows that the effects of condensation on the rate of change of the θ and q gradients are opposite in sign, but the absolute contributions to the tendency of the θ gradients are greater than those of the q gradients. This indicates that the NMPV generation is mainly dependent on the changes in the magnitude of the θ gradients (cf. Figs. 14d and 14h) if there are substantial differences in directions between the θ and q gradient vectors (e.g., Fig. 15). As indicated in the previous subsection, the orientations of the q gradient vectors typically change more rapidly than those of the θ gradient vectors, which is consistent with the frequently observed moist and/or dry air intrusion into the baroclinic zones.

As mentioned earlier, the large q and θ gradients associated with the NMPV generation are often found at or near the cyclone centers partly due to the presence of strong deformational flows. During the cyclone
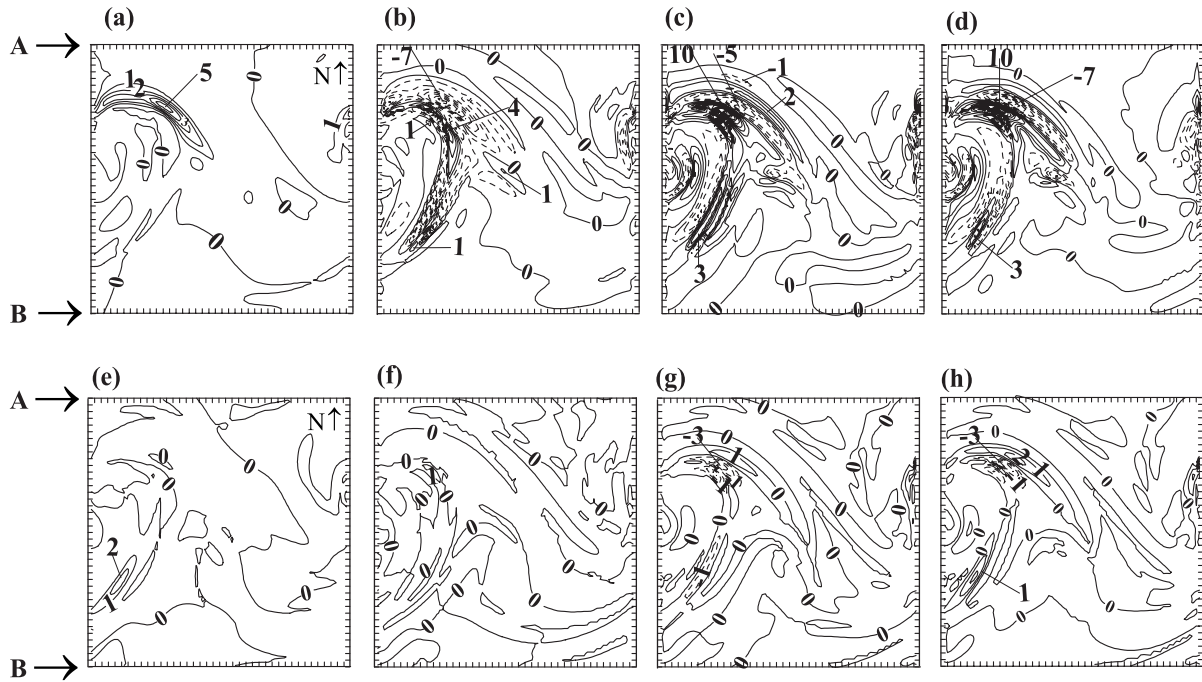
Fig. 14. Horizontal distribution of (a) the first term (confluence), (b) the second term (tilting), (c) the third term (latent heating), and (d) the sum of these three terms, at intervals of 1×10^{-9} K m^{-1} s^{-1}, on the right hand side of Eq. (9) for the control experiment at 48 h on the 757-hPa pressure surface. Note that the north-south window size is given by the line AB in Figs. 4b, 8b and 11b. The panels (e), (f), (g), and (h) are the same as (a), (b), (c), and (d), respectively, except for Eq. (10) at intervals of 1×10^{-12} m^{-1} s^{-1}.
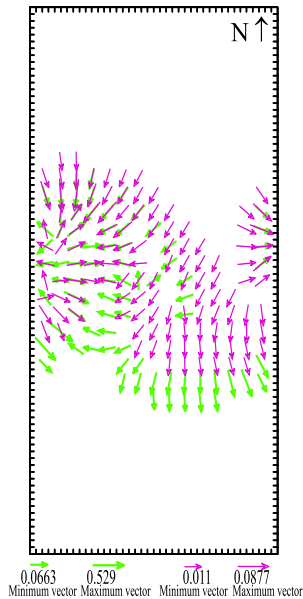

Fig. 15. Horizontal vectors of specific humidity gradients (green; each component scaled by a factor of 10^{-7} m^{-1}) and potential temperature gradients (in red; each component scaled by a factor of 10^{-3} K m^{-1}) on the 757-hPa pressure surface at 48 h of the control simulation.

deepening stage, the deformational flows alter the di-

rection and magnitude of the θ and q gradients, favoring the NMPV generation even when the q gradients are initially parallel to the θ gradients as in the control run. As a cyclone deepens, condensation occurring near the cyclone center tends to alter the θ and q gradient vectors, leading to the generation of NMPV. The enhanced cyclones may generate stronger vertical motion associated with latent heat release, causing the positive feedback between cyclogenesis and the NMPV generation. Although NMPV may occur at different regions of the extratropical cyclones as found by CC, the peak NMPV generally develops near the cyclone centers, which is one of the important characteristics of extratropical cyclones. This characteristic has been explored herein for the purpose of tracking the evolution of the surface cyclones.

4. Summary and conclusions

In this study, a prognostic equation relating the NMPV generation to the surface absolute vorticity is used to trace the evolution of surface cyclones. Its effectiveness is tested with idealized simulations of extratropical cyclones. It is found that the position of the peak NMPV coincides closely with that of the surface cyclone center during the development and mature

stages. This important characteristic provides a vital basis for tracing the movements of surface cyclones, serving as an alternative to the existing tracking methods. Two sensitivity experiments are conducted to examine the effects of initial moisture perturbations on tracking surface cyclones. Although MPV is sensitive to the initial moisture distributions, the peak NMPV appears to be always located near the cyclone center during the development and mature stages.

It is shown that the generation of NMPV depends on the magnitudes and orientations of the θ and q gradient vectors, which are determined by their initial conditions and the subsequent nonlinear advection and phase changes. The larger the initial NMPV source, the longer the time it will survive as a tracer of surface cyclones. NMPV tends to be generated in the neighborhood of condensation where the θ and q gradients are significantly enhanced. When NMPV appears in saturated regions at or near the cyclone centers, it may serve as a tracer of the surface cyclones for a longer time due to its conservative property.

The rates of changes of the θ gradient (F) and the q gradient (M) are calculated to quantify the generation of NMPV. It is shown that condensation, confluence, and tilting are important processes in determining the changes of both the θ and q gradients. The peak NMPV tends to be generated near the cyclone centers where the respective amplitude and direction of the θ and q gradients undergo significant changes as a result of the strong deformational flows and condensational influence. These changes occur near the cyclone center through the moist and/or dry air intrusion into the baroclinic zones.

In the future, more case studies need to be conducted to further examine the physical processes associated with cyclone tracks and the sensitivity of cyclone tracks to dynamic and thermodynamic processes from the MPV perspective.

REFERENCES

Anthes, R. A., E.-Y. Hsie, and Y.-H. Kuo, 1987: Description of the Penn State/NCAR Mesoscale Model Version 4 (MM4). NCAR Tech. Note, NCAR / TN-282, 66pp.

Betts, A. K., and F. J. Dugan, 1973: Empirical formula for saturation pseudoadiabats and saturation equivalent potential temperature. *J. Appl. Meteor.*, **12**, 731–732.

Browning, K. A., 1990: Organization of clouds and precipitation in extratropical cyclones. *Extratropical Cyclones. The Erik Palmen Memorial Volume*, C. W. Newton and E. Holopainen, Eds., Amer. Meteor. Soc., 132.

Cao, Z., and H.-R. Cho, 1995: Generation of moist potential vorticity in extratropical cyclones. *J. Atmos. Sci.*, **52**, 3263–3281.

Cao, Z., and G. W. K. Moore, 1998: A diagnostic study of moist potential vorticity generation in an extratropical cyclone. *Adv. Atmos. Sci.*, **15**, 152–166.

Cao, Z., R. E. Stewart, and W. D. Hogg, 2001: Extreme winter warming events over the Mackenzie basin: Dynamic and thermodynamic contributions. *J. Meteor. Soc. Japan*, **79**, 785–804.

Cao, Z., M. Wang, B. A. Proctor, G. S. Strong, R. E. Stewart, H. Ritchie, and J. E. Burford, 2002: On the physical processes associated with the water budget and discharge of the Mackenzie Basin during the 1994/1995 water year. *Atmos.-Ocean*, **40**, 125–143.

Cao, Z., and D. -L. Zhang, 2004: Tracking surface cyclones with moist potential vorticity. *Adv. Atmos. Sci.*, **21**, 830–835.

Cao, Z., P. Pellerin, and H. Ritchie, 2004: Verification of mesoscale modeling for the severe rainfall event over southern Ontario in May 2000. *Geophys. Res. Lett.*, **31**, L23108, doi:10.1029/2004GL020547.

Colle, B. A., and C. F. Mass, 1999: An observational and numerical study of a cold front interacting with the Olympic Mountains during COAST IOP5. *Mon. Wea. Rev.*, **127**, 1310–1334.

Davis, C. A., and K. A. Emanuel, 1991: Potential vorticity diagnosis of cyclogenesis. *Mon. Wea. Rev.*, **119**, 1929–1953.

Fraedrich, K., R. Bach, and G. Naujokat, 1986: Single station climatology of central European fronts: Number, time and precipitation statistics. *Contrib. Atmos. Phys.*, **59**, 54–65.

Gao, S., X. Li, and W.-K. Tao, 2004: A convective vorticity vector associated with tropical convection: A two-dimensional cloud-resolving modeling study. *J. Geophys. Res.*, **109**, D14106, doi:10.1029/2004JD004807.

Gyakum, J., 1983: On the evolution of the QE II storm. II: Dynamic and thermodynamic structure. *Mon. Wea. Rev.*, **111**, 1156–1173.

Gyakum, J., D.-L. Zhang, J. Witte, K. Thomas, and W. Wintels, 1996: CASP II and Canadian cyclones during the 1989-92 cold seasons. *Atmos.-Ocean*, **34**, 1–16.

Hoskins, B. J., M. E. McIntyre, and A. W. Robertson, 1985: On the use and significance of isentropic potential vorticity maps. *Quart. J. Roy. Meteor. Soc.*, **111**, 877–946.

Hsie, E.-Y., R. A. Anthes, and D. Keyser, 1984: Numerical simulation of frontogenesis in a moist atmosphere. *J. Atmos. Sci.*, **41**, 2581–2594.

Hu, Q., and E. R. Reiter, 1987: A diagnostic study of explosive cyclogenesis in the lee of the Rocky Mountains. *Meteor. Atmos. Phys.*, **36**, 161–184.

Huo, Z., D.-L. Zhang, and J. Gyakum, 1998: An application of potential vorticity inversion to improving the numerical prediction of the March 1993 superstorm. *Mon. Wea. Rev.*, **126**, 424–436.

Neiman, P. J., and M. A. Shapiro, 1993: The life cycle of an extratropical marine cyclone. Part I: Frontal-cyclone evolution and thermodynamic air-sea interaction. *Mon. Wea. Rev.*, **121**, 2153–2176.

Neiman, P. J., M. A. Shapiro, and L. S. Fedor, 1993: The life cycle of an extratropical marine cyclone. Part II: Mesoscale structure and diagnostics. *Mon. Wea. Rev.*, **121**, 2177–2199.

Petterssen, S., 1936: Contribution to the theory of frontogenesis. *Geofys. Publ.*, **11**, 1–27.

Reed, R. J., G. A. Grell, and Y.-H. Kuo, 1993: The ERICA IOP 5 storm. Part II: Sensitivity tests and further diagnosis based on model output. *Mon. Wea. Rev.*, **121**, 1595–1612.

Roebber, P. J., 1984: Statistical analysis and updated climatology of explosive cyclones. *Mon. Wea. Rev.*, **112**, 1577–1589.

Shapiro, M. A., and D. Keyser, 1990: Fronts, jet streams, and the tropopause. *Extratropical cyclones. The Erik Palmn Memorial Volume*, C. W. Newton and E. Holopainen, Eds., Amer. Meteor. Soc., 161–191.

Szeto, K. K., A. Tremblay, H. Guan, D. R. Hudak, R. E. Stewart, and Z. Cao, 1999: The mesoscale dynamics of freezing rain storms over eastern Canada. *J. Atmos. Sci.*, **56**, 1261–1281.

Thorpe, A. J., and S. A. Clough, 1991: Mesoscale dynamics of cold fronts: Structures described by dropsoundings in FRONTS 87. *Quart. J. Roy. Meteor. Soc.*, **117**, 903–941.

Uccellini, L. W., 1990: Processes contributing to the rapid development of extratropical cyclones. *Extratropical cyclones. The Erik Palmn Memorial Volume*, C. W. Newton and E. Holopainen, Eds., Amer. Meteor. Soc., 81–105.

Weldon, R. B., 1979: Satellite training course notes. Part IV. Cloud patterns and upper air wind field. United States Air Force, AWS/TR-79/003.

Zhang, G. J., 2003: Lagrangian study of cloud properties and their relationships to meteorological parameters over the U. S. Southern Great Plains. *J. Climate*, **16**, 2700–2716.